EAST EUROPEAN JOURNAL OF PHYSICS. 4. 527-536 (2025)
DOI:10.26565/2312-4334-2025-4-54 ISSN 2312-4334

EFFECT OF BORIC AND OXALIC ACID ON NUCLEATION MECHANISM, COMPOSITION, MORPHOLOGY AND STRUCTURE OF ELECTRODEPOSITED Ni FILMS

F.Z.K. Hamdi[1]*, A. Rahmani[1,2], A. Hamdi[1]
[1]*Laboratory of Physical Chemistry of Materials (LPCM), Faculty of Sciences, University of Amar Telidji, 03000, Laghouat, Algeria*
[2]*Laboratory MONARIS, UMR 8233, Sorbonne Université, 4 place Jussieu, 75005 Paris, France*
**Corresponding Author e-mail: f.hamdi@lagh-univ.dz*
Received August 23, 2025; revised October 16, 2025; accepted October 23, 2025

Nickel thin films were electrodeposited onto copper substrates at room temperature using an aqueous electrolyte containing nickel sulfate, nickel chloride, and sodium sulfate. The effects of two additives (boric acid and oxalic acid) on the nucleation mechanism, crystallographic structure, surface morphology, and chemical composition of the resulting Ni films were systematically investigated using cyclic voltammetry (CV), chronoamperometry (CA), X-ray diffraction (XRD), scanning electron microscopy (SEM), and energy-dispersive X-ray spectroscopy (EDS). CV analysis revealed that the presence of additives shifted the cathodic peak potentials toward more negative values, suggesting an inhibition effect on nickel reduction. Chronoamperometric studies confirmed that Ni deposition followed a three-dimensional instantaneous nucleation mode, unaffected by the additives. XRD patterns showed that all Ni films had a face-centered cubic (FCC) structure with strong (111) orientation, while SEM images indicated denser and more homogeneous surface morphology in the presence of additives. EDS analysis confirmed the presence of Ni in all samples.
Keywords: *Nickel; Electrodeposited; Additives; Boric acid; Oxalic acid; Nucleation*
PACS: 81.15.Pq; 81.10.Aj; 68.55.-a; 68.35.B-

1. INTRODUCTION

Nickel (Ni) coatings are widely used in various industrial applications, including catalysis [1], electronic components [2], decorative purposes [3], and corrosion protection, due to their excellent properties such as oxidation resistance [4], high corrosion and wear resistance [5−8], and good optical, magnetic, and mechanical characteristics [9]. Several physical and chemical methods have been employed to synthesize Ni thin films, including chemical vapor deposition (CVD) [10], the sol–gel method [11], spray pyrolysis [12], sputtering [13], thermal evaporation [14], and electrodeposition [15]. Among these, electrodeposition is widely used due to its simplicity, low cost, high efficiency [16,17], and low processing temperature [18]. In electrodeposition, the properties of the resulting films are influenced by several parameters, including deposition time, current density, applied potential, electrolyte temperature, pH, bath composition, stirring speed, and the use of additives [19–21]. Small amounts of additives in the electrolyte have been shown to significantly influence the microstructure, morphology, and overall quality of the deposit. These characteristics are closely linked to the nucleation and growth mechanisms occurring during the initial stages [2].

In this study, we aim to investigate the effect of two additives (boric acid and oxalic acid) on the nucleation and growth mechanisms of nickel electrodeposited on a copper substrate at room temperature. Cyclic voltammetry (CV) and chronoamperometry (CA) were employed to analyze the electrochemical behavior. The surface morphology, chemical composition, and crystal structure of the resulting films were also characterized using scanning electron microscopy (SEM), energy-dispersive X-ray spectroscopy (EDS), and X-ray diffraction (XRD), respectively.

2. MATERIALS AND METHODS

Nickel films were deposited at room temperature using a basic three-electrode electrochemical setup, linked to a PGZ402 potentiostat/galvanostat (Radiometer Analytical). The system included a saturated calomel electrode (SCE) as the reference, a platinum foil as the counter, and a copper disc (1.50 cm × 1.00 cm) acting as the working electrode. Before any deposition, the copper samples were polished by hand using silicon carbide papers ranging from 1200 to 2000 grit. After polishing, the surface was cleaned in acetone, rinsed with distilled water, and left to dry in air. No extra surface treatment was done. All electrolytes were freshly prepared using deionized water and analytical-grade chemicals. The pH of each bath was adjusted to around 2.8 using either NaOH or H_2SO_4. Table 1 lists the full composition of the bath and the main deposition parameters.

To investigate the electrodeposition process, we used both cyclic voltammetry (CV) and chronoamperometry (CA). CV scans were run between 0 and –1.4 V vs SCE, with a scan rate fixed at 20 mV/s.

For surface and structural analysis, ESEM (Thermo Scientific™ Quattro S) was used in combination with EDS to examine the morphology and composition of the films. Structural information was obtained using X-ray diffraction (XRD), performed on a PANalytical Empyrean diffractometer operating at 40 kV and 30 mA. Measurements used Cu Kα radiation (λ = 1.54060 Å) with a Ni filter. The 2θ range was set from 30° to 100°, with a scan step of 0.02°/s.

Cite as: F.Z.K. Hamdi, A. Rahmani, A. Hamdi, East Eur. J. Phys. 4, 527 (2025), https://doi.org/10.26565/2312-4334-2025-4-54

Table 1. The electrolyte compositions and plating parameters

Bath composition		Plating parameters	
Chemicals	**Concentrations [g L^{-1}]**		
$NiSO_4 \cdot 6H_2O$	60		
$NiCl_2.6H_2O$	8.2	pH	≈ 2.8
Na_2SO_4	0.5	Room temperature	25°C
		Room temperature	5 min
Additives		Deposition potential	-1000 mV
$C_2H_2O_4.2H_2O$	0.84		
H_3BO_3	24.7		

3. RESULTS AND DISCUSSIONS

3.1. Cyclic voltametric studies

The cyclic voltammetry technique is widely employed in electrochemistry, revealing electrode/electrolytic solution behavior and enabling the prediction of ideal conditions for the metal ions electrodeposition mechanism [16]. Figure 1 shows the CV curves of nickel thin films electrodeposited onto a copper substrate at room temperature, both in the absence and presence of additives. The potential was swept from 0 V vs. SCE toward the cathodic side, down to -1.4 V vs. SCE, and then reversed back to the starting point, with a scan rate set at 20 mV/s.

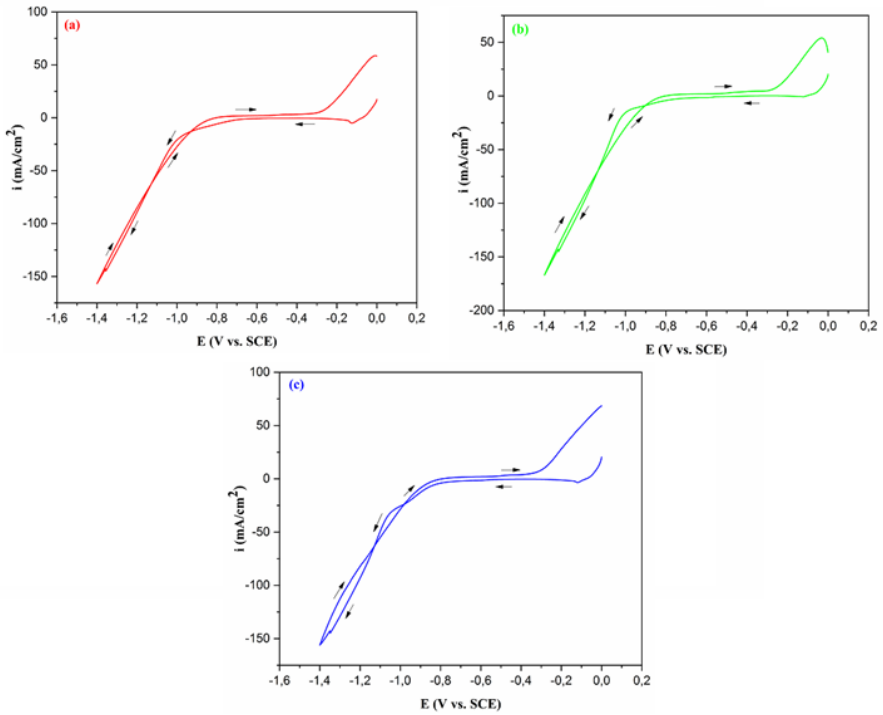

Figure 1. Cyclic voltammograms for copper substrate in solution containing: (a) 60 g L^{-1} $NiSO_4 \cdot 6H_2O$, 8.2 g L^{-1} $NiCl_2.6H_2O$ and 0.5 g L^{-1} Na_2SO_4 (b) 60 g L^{-1} $NiSO_4 \cdot 6H_2O$, 8.2 g L^{-1} $NiCl_2.6H_2O$, 0.5 g L^{-1} Na_2SO_4 and 24.7 g L^{-1} H_3BO_3 and (c) 60 g L^{-1} $NiSO_4 \cdot 6H_2O$, 8.2 g L^{-1} $NiCl_2.6H_2O$, 0.5 g L^{-1} Na_2SO_4 and 0.84 g L^{-1} $C_2H_2O_4.2H_2O$. (T = 25°C, v = 20 mVs^{-1})

In the additive-free bath (Figure 1(a)), the reduction of Ni^{2+} ions begins at around -0.70 V, following the reaction shown in Equation (1). As the potential becomes more negative, a noticeable rise in current density is observed, mainly due to the concurrent hydrogen evolution reaction, described by Equation (2):

$$Ni^{2+} + 2e^- \rightarrow Ni \quad (1)$$

$$2H^+ + 2e^- \rightleftharpoons H_2 \quad (2)$$

During the return scan, the dissolution of metallic Ni to Ni^{2+} appears an potential of -0.260 V.

With the addition of boric acid in the electrolyte (Figure 1(b)), the reduction of nickel begins at E = -0.980 V. In anodic part, an anodic peak observed at E= -0.030 V is due to the oxidation of the nickel deposited during the cathodic part according to Eq. (3).

$$Ni \rightarrow Ni^{2+} + 2e \quad (3)$$

When oxalic acid is added (Figure 1(c)), the reduction of nickel starts at a potential of approximately -0.820 V, and the dissolution of Ni occurs at about -0.304 V.

The introduction of additives (boric and oxalic acid) in the bath solution shifted the cathodic peak potential negatively. This indicates that these additives inhibited nickel electrodeposition, and the force of the inhibition effect followed this order: H_3BO_3 > $C_2H_2O_4$. The hydrogen reaction occurs at a more negative potential in the presence of additives, indicating that boric and oxalic acid had a significant inhibition effect on hydrogen reduction.

The presence of the crossover in the cyclic voltammograms (CVs) indicates the existence of a nucleation and growth process [22].

3.2. Chronoamperometry

3.2.1. Current density-time curves

To study the effect of additives on a Ni electrodeposition nucleation/growth mechanism, chronoamperometry was employed. Figure 2 illustrates the current density transient curves of nickel thin films electrodeposited on copper substrate at different potentials in the absence and presence of additives. For all films, the transients have the same form. These curves show three parts. In the first part, the current density decreases abruptly due to the charge of the double layer and the formation of the first germs of Ni on the electrode surface. Then, in the second part, the current density increases, reaching a maximum value, imax, at a maximum time, tmax, due to the growth of Ni nuclei. Finally, in the last part, the current density decreases and stabilizes as the deposition potentials increase, indicating that the growth process of nickel is controlled by the diffusion regime [23,24]. We can conclude that these current–time transients are a typical characteristic of a three-dimensional nucleation with diffusion-controlled growth [1].

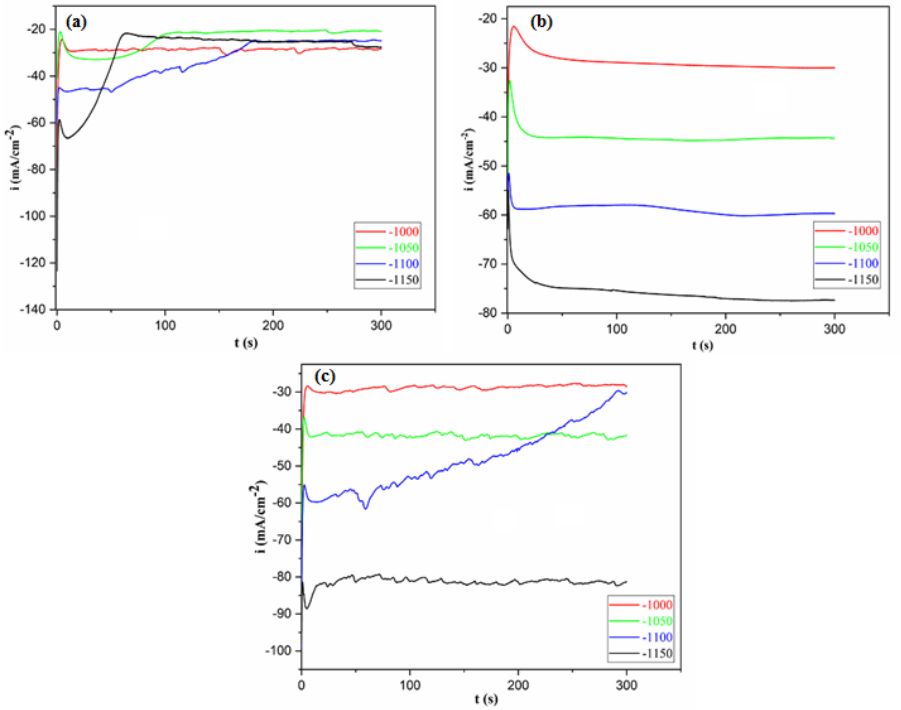

Figure 2. Typical current transient curves of Ni films electrodeposited on Cu substrate at different potentials in solution containing: (a) 60 g L^{-1} $NiSO_4{\cdot}6H_2O$, 8.2 g L^{-1} $NiCl_2.6H_2O$ and 0.5 g L^{-1} Na_2SO_4 (b) 60 g L^{-1} $NiSO_4{\cdot}6H_2O$, 8.2 g L^{-1} $NiCl_2.6H_2O$, 0.5 g L^{-1} Na_2SO_4 and 24.7 g L^{-1} H_3BO_3 and (c) 60 g L^{-1} $NiSO_4{\cdot}6H_2O$, 8.2 g L^{-1} $NiCl_2.6H_2O$, 0.5 g L^{-1} Na_2SO_4 and 0.84 g L^{-1} $C_2H_2O_4.2H_2O$.(t= 5 min, T= 25°C)

3.2.2. Nucleation mechanisms

To further understand the nucleation mechanism of nickel deposition, the mathematical model developed by Scharifker and Hills (SH) [25] was used. According to this model, the nucleation mechanism includes instantaneous and progressive 3D nucleation [20]. The mechanism is described by the following Eq. (4) and (5) [26]:

Instantaneous nucleation:

$$i^2/i_{max}^2 = 1.9542(t/t_{max})^{-1}[1 - \exp(-1.2564(t/t_{max}))]^2 \quad (4)$$

Progressive nucleation:

$$i^2/i_{max}^2 = 1.2254(t/t_{max})^{-1}[1 - \exp(-2.3367(t^2/t_{max}^2))]^2 \quad (5)$$

where i_{max} and t_{max} are the maximum current density and the corresponding time, respectively.

Figures 3, 4, and 5 represent the dimensionless theoretical $(i/i_{max})^2$ vs (t/t_{max}) plots resulting from Eq. (4) and (5), and experimental current density transients during the electrodeposition of nickel on a copper substrate at different

potentials in the absence and presence of additives in the electrolyte. It can be seen that at $(t/t_{max}) \leq 1$, the experimental plots at different applied potentials (with and without additives) tend to the instantaneous nucleation model. Hence, the electrodeposition of nickel on copper substrate nucleation follows the 3D instantaneous nucleation mode at short time [23,27], which indicates that the addition of additives did not change the nucleation mechanism of the nickel. For (t/tm > 1, the experimental curves show a negligible difference from the Scharifker model. This difference is related to the proton reduction on the copper surface [28].

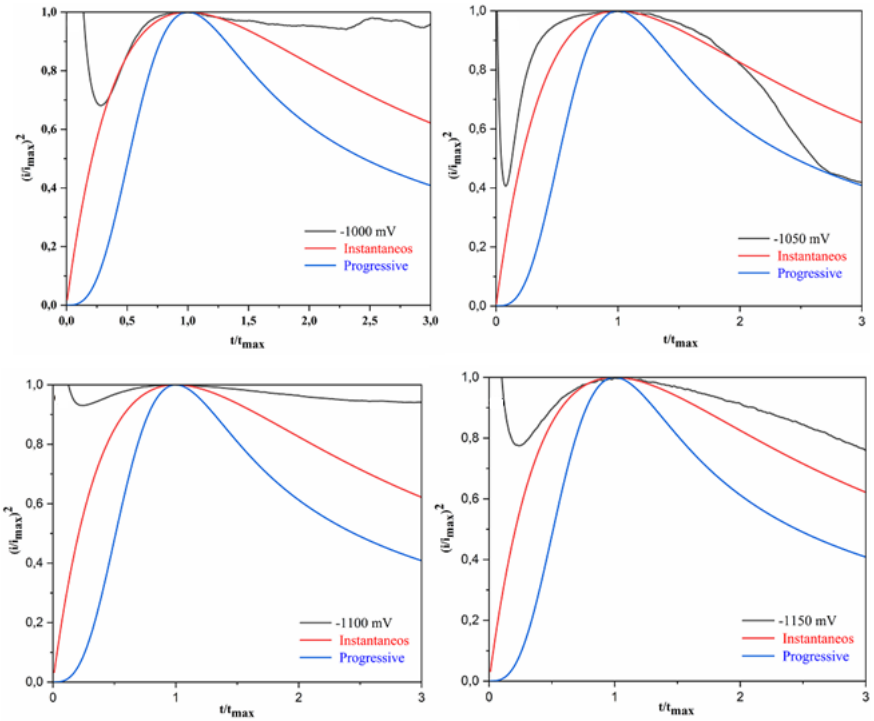

Figure 3. Comparison of theoretical non-dimensional $(i/i_{max})^2$ vs (t/t_{max}) plots for instantaneous nucleation from Eq. (4) and progressive nucleation from Eq. (5) to experimental current density transients for the electrodeposition of nickel on a copper substrate at different potentials in the absence of additives

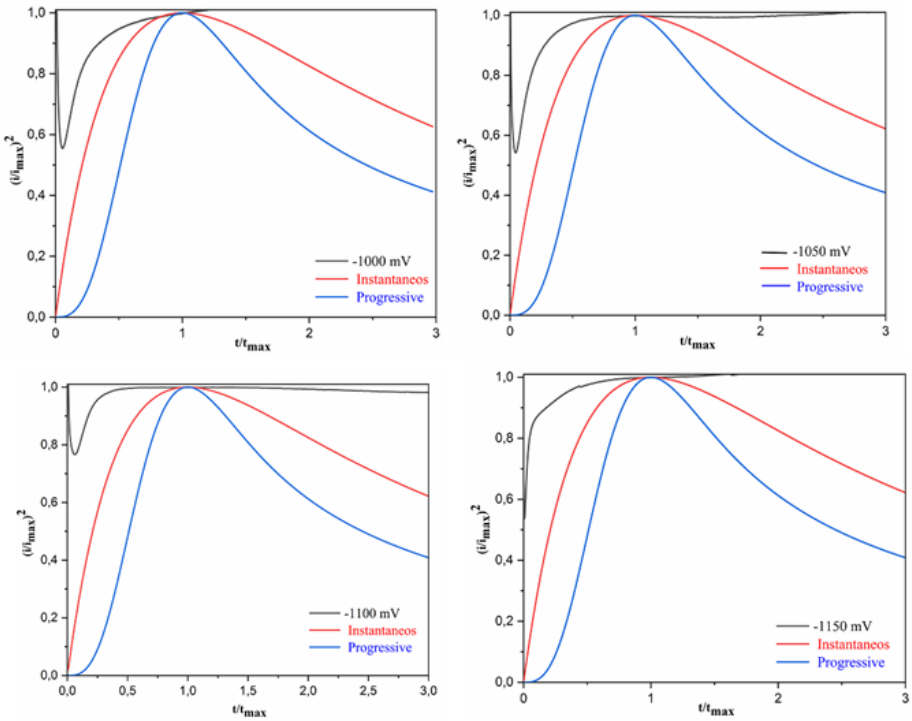

Figure 4. Comparison of theoretical non-dimensional $(i/i_{max})^2$ vs (t/t_{max}) plots for instantaneous nucleation from Eq. (4) and progressive nucleation from Eq. (5) to experimental current density transients for the electrodeposition of nickel on a copper substrate at different potentials in the presence of 24.7 g L^{-1} H_3BO_3 in the bath

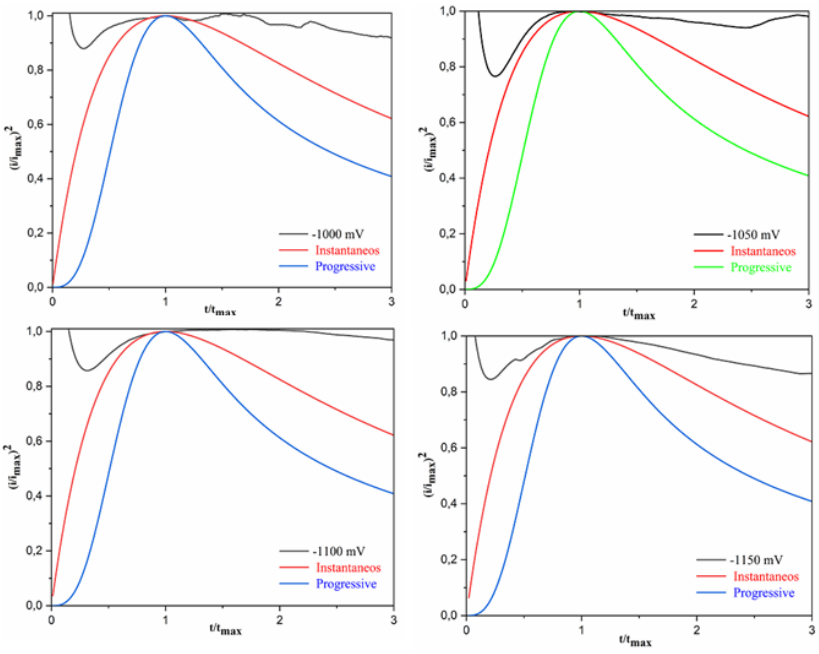

Figure 5. Comparison of theoretical non-dimensional $(i/i_{max})^2$ vs (t/t_{max}) plots for instantaneous nucleation from Eq. (4) and progressive nucleation from Eq. (5) to experimental current density transients for the electrodeposition of nickel on a copper substrate at different potentials in the presence of 0.84 g L^{-1} $C_2H_2O_4$ in the bath

3.2.3. Kinetic parameters of the nickel electrodeposition

According to Scharifker and Hills model, the diffusion coefficient (D_{inst}), the number of active nucleation sites (N_0), and the nucleation rate (A) can be determined from the current density transients using the following equations [29,30]:

$$D = \frac{i_{max}^2 t_{max}^2}{0.1629(nFC)^2} \quad (6)$$

$$N_0 = 0.065\left(\frac{8\pi CM}{\rho}\right)^{-1/2}\left(\frac{nFC}{i_{max}t_{max}}\right)^2 \quad (7)$$

$$A = N_0\pi\left(\frac{8\pi CM}{\rho}\right)^{1/2} D \quad (8)$$

where n is the number of transferred electrons, M is the atomic weight, t is time, F is the Faraday constant (96500 C/mol), C is the concentration of the electroactive species (mol/l), and ρ is the density of the Ni deposit.

Values of t_{max}, i_{max}, D, A and N_0 at different potentials are shown in Table 2. It is clear that as the applied potential increase, the maximum current density increases, and the maximum time (tmax) decreases. This feature is typical of three-dimensional electrochemical nucleation and growth of a new phase governed by diffusion control. The number of active nucleation sites (N_0) increases in the presence and absence of additives in the bath, but the nucleation rate (A) decreases. These results are characteristic for 3D instantaneous nucleation process.

Table 2. The values of t_{max}, i_{max}, D, A, and N_0 for electrodeposition of Ni in the absence and presence of additives at deposition potentials obtained from current density transient curves using Eq. (6), (7) and (8)

Additive Composition	E (mV)	t_{max} (s)	$-i_{max}$ (mA cm^{-2})	D (cm^2 s^{-1})	A (s^{-1})	N_0 (cm^{-2})
Without additive	-1000	15.50	29.45	$4.99.10^{-4}$	1.26	$1.23.10^2$
	-1050	36.30	32.97	$0.34.10^{-4}$	0.01	$0.17.10^2$
	-1100	9.30	46.63	$4.50.10^{-4}$	1.23	$1.33.10^2$
	-1150	9.40	66.65	$9.41.10^{-4}$	1.24	$0.64.10^2$
With boric acid	-1000	100.90	28.94	0.02	0.82	$0.02.10^2$
	-1050	40.30	44.28	$0.76.10^{-4}$	0.01	$0.07.10^2$
	-1100	15.18	58.83	$0.19.10^{-4}$	0.01	$0.31.10^2$
	-1150	58.80	74.99	0.04	0.83	$0.01.10^2$
With oxalic acid	-1000	20.70	30.24	$9.39.10^{-4}$	1.20	$0.62.10^2$
	-1050	9.60	42.17	$3.93.10^{-4}$	1.24	$1.53.10^2$
	-1100	8.40	59.52	$5.99.10^{-4}$	1.23	$1.00.10^2$
	-1150	4.70	88.57	$4.15.10^{-4}$	1.24	$1.45.10^2$

3.3. Structure analysis

The structural properties of the nickel deposit were determined by (XRD) measurements. Figure 6 exhibited the X-ray diffraction (XRD) patterns ($40^\circ \leq 2\theta \leq 100^\circ$) of Ni electrodeposited on copper substrate in the absence and presence of different additives at 25.0 ºC at the deposition potential of -1000 mV. The results revealed that the obtained films are polycrystalline structure. All films show diffraction peaks located at $2\theta = 43.91^\circ$, 50.97°, 74.43° and 90.43°, corresponding to (111), (200), (220) and (311) crystalline planes of Cu substrate according to ICDD card no. 00-003-1018, respectively. However, the peaks observed at around 44.03°, 51.10° and 79.76°, corresponding to (111), (200) and (220) reflections planes of Ni (ICSD n° 01-089-7128 and ICSD n° 01-088-2326), as indicated by the face-centered cubic (FCC) structure of nickel. The addition of additives shifted slightly these peaks toward lower 2θ values. The (111) plane is the stronger, indicating that it is the preferential orientation. In the presence of boric acid in the bath, the intensity of this peak increases. The XRD pattern revealed two distinct diffraction peaks at $2\theta = 66.53°$ and 71.07°, which correspond to the (411) and (332) planes of tetragonal Cu_4O_3 (ICSD n° 01-083-1665). This mixed-valence copper oxide phase most likely developed as a result of partial oxidation of exposed copper substrate regions where nickel electrodeposition was not complete. Local oxidation may have resulted from the presence of microbubbles created by hydrogen evolution during the deposition process, which prevented uniform Ni coverage. Interestingly, samples with continuous nickel films did not exhibit these Cu_4O_3 related peaks, demonstrating that complete surface coverage successfully shields the underlying copper from oxidation.

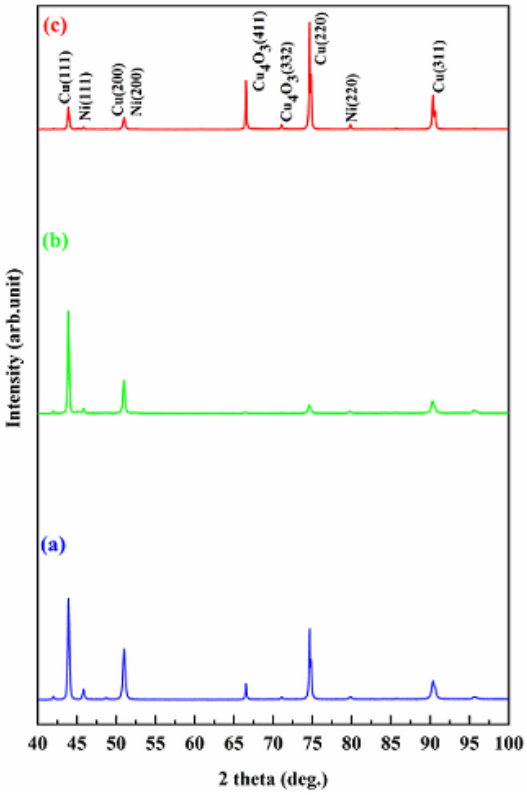

Figure 6. X-ray diffractograms of Ni films electrodeposited at -1000 mV and t= 5 min in solution containing: (a) 60 g L^{-1} $NiSO_4 \cdot 6H_2O$, 8.2 g L^{-1} $NiCl_2.6H_2O$ and 0.5 g L^{-1} Na_2SO_4 (b) 60 g L^{-1} $NiSO_4 \cdot 6H_2O$, 8.2 g L^{-1} $NiCl_2.6H_2O$, 0.5 g L^{-1} Na_2SO_4 and 24.7 g L^{-1} H_3BO_3 and (c) 60 g L^{-1} $NiSO_4 \cdot 6H_2O$, 8.2 g L^{-1} $NiCl_2.6H_2O$, 0.5 g L^{-1} Na_2SO_4 and 0.84 g L^{-1} $C_2H_2O_4.2H_2O$

The lattice parameters were calculated using XRD data as follows [30]:

$$a = d_{hkl}\sqrt{h^2 + k^2 + l^2} \tag{9}$$

and

$$\frac{1}{d_{hkl}^2} = \frac{4}{3}\left(\frac{h^2+hk+k^2}{a^2}\right) + \frac{l^2}{c^2} \tag{10}$$

where d_{hkl} is interplanar spacing, (h k l) are Miller indices, a and c are the lattice parameters, respectively [18]. The average crystallite size (D) was evaluated by Debye Sheerer's equation [32]:

$$D = \frac{K\,\lambda}{\beta\cos\theta} \tag{11}$$

where K is the Scherrer constant (= 0.94), λ is the X-ray wavelength (λ = 1.54060 Å), β is the full width at half maximum (FWHM) value, and θ is the Bragg diffraction angle.

The dislocation density (δ) was estimated by following relation [33]:

$$\delta = \frac{1}{D^2} \tag{12}$$

The microstrain (ε) was also calculated using the following formula [34]:

$$\varepsilon = \frac{\beta \cos\theta}{4} \tag{13}$$

The FWHM values, the crystalline sizes, diffraction angle 2θ, the microstrain and dislocation densities of the Ni thin films were mesured using the (111) diffraction peak are presented in Table 3. It is clear that the introduction of boric and oxalic acid in the electrolyte decreases the FWHM. In addition, the lattice parameters (a) and the crystallite size of the films increased in the presence of additives. Thus, it can be said that the crystallinity of coating is extremely affected by the addition of additives on the bath. The obtained results show that the microstrain and dislocation densities values of the Ni films were reduced with the addition of additives.

Table 3. Structural parameters of the nickel thin films

Ni Films	FWHM	2θ (°)	a (Å)	(hkl)	d_{hkl} (Å)	D (nm)	δ×10^{-3} (Lines/m^2)	ε ×10^{-2}
without additives	0,19	44.03	3.567	(111)	2,0599	10.598	8.91	3.41
with H_3BO_3	0,13	44.01	3.569	(111)	2,0609	15.488	4.17	2.34
with $C_2H_2O_4$	0,16	44.02	3.568	(111)	2,0604	12.583	6.32	2.88

3.4. SEM analysis

The surface morphology of the e nickel films was examined using high-resolution SEM imaging at 50,000× magnification, and the results are presented in Figure 7. The three micrographs correspond to Ni films deposited at room temperature and –1000 mV, obtained without any additive (Figure 7(a)), with boric acid (Figure 7(b)), and with oxalic acid (Figure 7(c)).

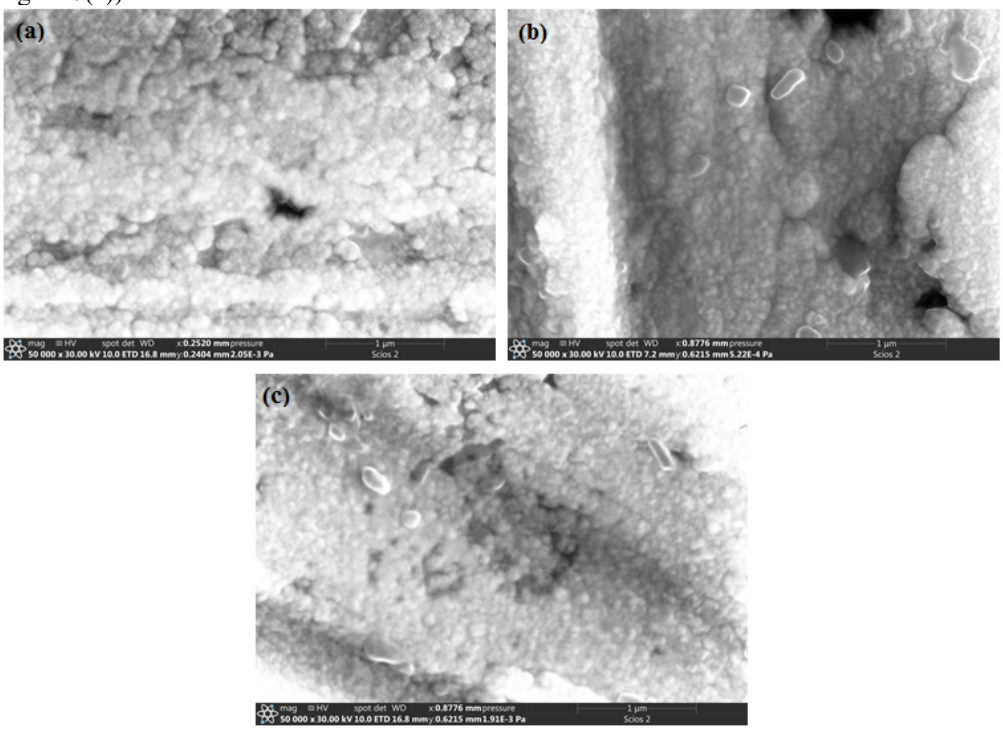

Figure 7. SEM micrographs of nickel thin films electrodeposited at -1000 mV and t= 5 min in solution containing: (a) 60 g L^{-1} $NiSO_4{\cdot}6H_2O$, 8.2 g L^{-1} $NiCl_2.6H_2O$ and 0.5 g L^{-1} Na_2SO_4 (c) 60 g L^{-1} $NiSO_4{\cdot}6H_2O$, 8.2 g L^{-1} $NiCl_2.6H_2O$, 0.5 g L^{-1} Na_2SO_4 and 24.7 g L^{-1} H_3BO_3 and (e) 60 g L^{-1} $NiSO_4{\cdot}6H_2O$, 8.2 g L^{-1} $NiCl_2.6H_2O$, 0.5 g L^{-1} Na_2SO_4 and 0.84 g L^{-1} $C_2H_2O_4.2H_2O$

Without additives (Figure 7(a)), the film shows a porous, kind of rough surface, with spherical grains that aren't packed tightly and have different sizes. Many voids and pits are visible, probably due to hydrogen bubbles that got stuck during deposition. This interuption in the growth causes poor coverage and uneven distribution over the copper surface, which also means nucleation wasn't very efficient.

With the addition of boric acid (Figure 7(b)), the surface looks clearly better. The film is more compact and much smoother, grains are finer too. No major cracks or flaws were observed, and the substrate seems fully covered. Most likely, boric acid helps keeping the local pH steady and also minimizes hydrogen evolution, which makes the whole process of deposition more controlled.

As for the film with oxalic acid (Figure 7(c)), it also seems denser, although the grains here are a bit larger and less packed compared to the boric acid one. Still, the surface stays relatively smooth, and there's no serious defect you can spot. This might be because oxalic acid interacts with Ni^{2+} ions differently, maybe slowing down the reaction by forming weak complexes, which changes how the film grows.

Overall, adding these acids to the bath significantly improves the coating. Both boric and oxalic acid enhanced the surface coverage and adhesion, but boric acid led to a film that's clearly more uniform and compact.

3.5. EDS analysis

EDS (Energy dispersive Xray spectroscopy) was used to assess the elemental composition of the Ni films deposited on copper substrate under different bath conditions, and the results are summarized in Figure 8(a–c).

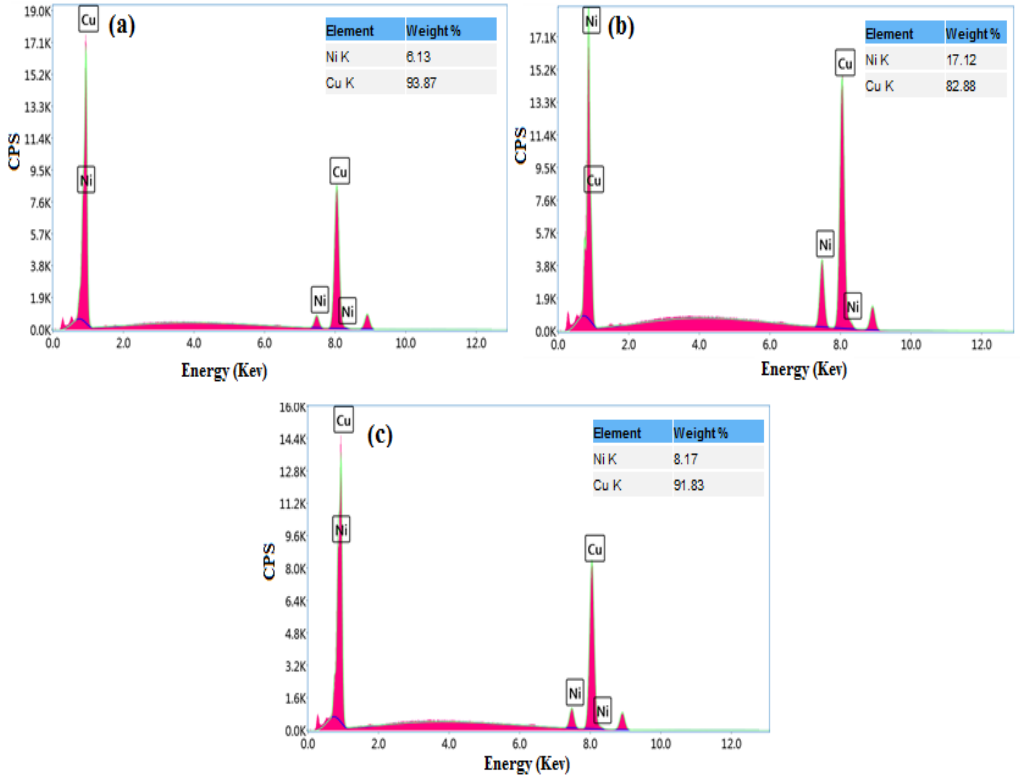

Figure 8. EDS spectrum of nickel coatings electrodeposited at -1000 mV and t= 5 min in solution containing: (a) 60 g L^{-1} $NiSO_4{\cdot}6H_2O$, 8.2 g L^{-1} $NiCl_2.6H_2O$ and 0.5 g L^{-1} Na_2SO_4 (c) 60 g L^{-1} $NiSO_4{\cdot}6H_2O$, 8.2 g L^{-1} $NiCl_2.6H_2O$, 0.5 g L^{-1} Na_2SO_4 and 24.7 g L^{-1} H_3BO_3 and (e) 60 g L^{-1} $NiSO_4{\cdot}6H_2O$, 8.2 g L^{-1} $NiCl_2.6H_2O$, 0.5 g L^{-1} Na_2SO_4 and 0.84 g L^{-1} $C_2H_2O_4.2H_2O$

Each spectrum displays characteristic peaks for Ni and Cu, indicating the coexistence of both elements in the analyzed area. The relative weight percentages give further insight into how effectively the nickel coating formed in each case.

In the sample without any additives (Figure 8(a)), the nickel content is notably low, with Ni accounting for only about 6.13 wt%. This weak signal is consistent with the SEM observations, which show poor surface coverage. The dominant Cu signal (93.87 wt%) suggests that the underlying copper substrate is largely exposed, indicating either a very thin Ni layer or incomplete film formation. This aligns well with the porous and uneven morphology previously observed.

When boric acid is used in the electrolyte (Figure 8(b)), the nickel content significantly increases to 17.12 wt%, while the copper signal drops to 82.88 wt%. This suggests a much thicker and more complete nickel deposit on the substrate. The improved Ni/Cu ratio is in line with the denser, more uniform coating observed in the SEM image (Fig. 5b), confirming that boric acid promotes more efficient metal deposition and better surface coverage.

The film deposited from the bath containing oxalic acid (Figure 8(c)) shows an intermediate composition. The nickel weight percentage rises slightly to 8.17 wt%, higher than the additive-free condition but still significantly lower than with boric acid. This implies partial improvement in Ni deposition and coverage, though not as effective as with boric acid. The Cu peak remains relatively strong (91.83 wt%), reflecting limited shielding of the substrate. This result also matches the SEM image in Fig. 5c, where the surface appeared smoother but with larger grains and less compact packing.

Overall, the EDX results confirm that both boric and oxalic acid additives enhance nickel deposition efficiency. However, boric acid appears more effective in promoting thick, uniform coatings with higher Ni content, likely due to its buffering capacity and suppression of parasitic hydrogen evolution.

4. CONCLUSIONS

In this paper, nickel films have been successfully prepared on copper substrates using the electrodeposition method. The effect of the additives (boric acid and oxalic acid) on the nickel nucleation process, surface morphologies, chemical composition, and crystal structure was investigated. The (CV) analysis showed that the electrodeposition of Ni has been started at potential of approximately -0.70 V vs SCE and the presence of additives in the solution shifted negatively the cathodic peak potential. The (CA) analysis revealed that the electrochemical deposition of Ni followed the 3D instantaneous nucleation process and the presence of additives in the electrolyte did not affect the nucleation mechanism of Ni. XRD measurements showed that all nickel electrodeposited films had the face-centered cubic (FCC) structure with a (111) preferential orientation. In the presence of boric acid in the bath, the intensity of this peak increases. SEM analysis indicated that the thin films obtained from the solution containing additives exhibit good adhesion to copper substrates with a denser crystal size. EDS analysis confirmed the presence of Ni in all coatings.

ORCID

F.Z.K. Hamdi, https://orcid.org/0000-0001-9370-7715

REFERENCES

[1] A. Sahlaoui, Y. Lghazi, B. Youbi, M. Ait Himi, J. Bahar, C. El Haimer, A. Aynaou, *et al*., Moroccan Journal of Chemistry, **11**, 541 (2023). https://doi.org/10.48317/IMIST. PRSM/morjchem-v11i2.36809
[2] F. Zhang, S. Liu, and F. Wang, RSC advances, **12**, 11052 (2022). https://doi.org/10.1039/D1RA08926A
[3] S. Elsharkawy, D. Kutyła, and P. Żabiński, Coatings, **14**, 1459 (2024). https://doi.org/10.3390/coatings14111459
[4] X. Wang, G. Wang, W. Wang, X. Liu, Y. Liu, Y. Jin, and Y. Zhang, Journal of Alloys and Compounds, **1032**, 181014 (2025). https://doi.org/10.1016/j.jallcom.2025.181014
[5] H.F. Alesary, S. Cihangir, A.D. Ballantyne, R.C. Harris, D.P. Weston, A.P. Abbott, and K.S. Ryder, Electrochimica Acta, **304**, 118 (2019). https://doi.org/10.1016/j.electacta.2019.02.090
[6] S. Umrao, J. Jeon, S.M. Jeon, Y.J. Choi, and S. Lee, Nanoscale, **9**, 594 (2017). https://doi.org/10.1039/C6NR07240B
[7] B. Abedini, N.P. Ahmadi, S. Yazdani, and L. Magagnin, Transactions of Nonferrous Metals Society of China, **30**, 548 (2020). https://doi.org/10.1016/S1003-6326(20)65234-7
[8] Y. Xu, H. Jiao, M. Wang, and S. Jiao, Journal of Alloys and Compounds, **779**, 22 (2019). https://doi.org/10.1016/j.jallcom.2018.11.232
[9] K.D.M. Abro, A. Sanou, and E.K.I. Kwa-Koff, American Journal of Physical Chemistry, **13**, 1 (2024). https://doi.org/10.11648/j.ajpc.20241301.11
[10] E. Bouabdalli, M. El Jouad, T. Garmim, A. Louardi, B. Hartiti, M. Monkade, S. Touhtouh, and A. Hajjaji, Materials Science and Engineering: B. 286, 116044 (2022), https://doi.org/10.1016/j.mseb.2022.116044
[11] A. Shamim, Z. Ahmad, S. Mahmood, U. Ali, T. Mahmood and Z. Nizami, Open Journal of Chemistry, **2**, 16 (2019). https://www.doi.org/10.30538/psrp-ojc2019.0009
[12] A. Rahmani, L. Remache, M. Guendouz, N. Lorrain, A. Djermane, and L. Hadjeris, Surface Review and Letters, **29**, 2250039 (2021). https://doi.org/10.1142/S0218625X22500391
[13] F. Lekmine, I. Zidani, A. Chala, and A. Gana, Journal of nano- and electronic physics, **14**, 06022-1 (2022), https://doi.org/10.21272/jnep.14(6).06022
[14] N. Guermat, W. Daranfed, I. Bouchama, and N. Bouarissa, Journal of Molecular Structure, **1225**, 129134 (2021). https://doi.org/10.1016/j.molstruc.2020.129134
[15] G. Qadr, M.I. Awad, K. Haji, J.A. Jumaa, and H.H. Abdallah, Journal of Molecular Liquids, **378**, 121584 (2023). https://doi.org/10.1016/j.molliq.2023.121584
[16] C. El Haimer, Y. Lghazi, J. Bahar, B. Youbi, M. Ait Himi, A. Ouedrhiri, A. Aynaou, and I. Bimaghra, Materials Today: Proceedings, **66**, 37 (2022), https://doi.org/10.1016/j.matpr.2022.03.107
[17] X. Fu, C. Zhan, R. Zhang, B. Wang, H. Sun, and J. Sun, Journal of Solid State Electrochemistry, **26**, 2713 (2022). https://doi.org/10.1007/s10008-022-05282-z
[18] S. Saha, M. Johnson, F. Altayaran, Y. Wang, D. Wang, and Q. Zhang, Electrochem. **1**, 286 (2020). https://doi.org/10.3390/electrochem1030019
[19] I.M. Beker, F.B. Dejene, L.F. Koao, J.J. Terblans, S.Z. Werta, and A.U. Yimamu, Journal of Electronic Materials, **54**, 6575 (2025). https://doi.org/10.1007/s11664-025-12082-4
[20] L. Yuan, J. Chen, J. Zhang, and L. Sun, Crystals, **12**, 43 (2021), https://doi.org/10.3390/cryst12010043
[21] X. Wu, X. Zhao, P. Lin, C. Tan, C. Wang and W. Chen, Journal of Materials Research and Technology. **36**, 1789-1801 (2025), https://doi.org/10.1016/j.jmrt.2025.03.212
[22] F.Z. Hamdi, A. Hamdi, S. Khenchoul, A. Rahmani, A. Cheriet, L. Aissani and A. Alhussein, Journal of the Indian Chemical Society. **99**, 100498-100503 (2022), https://doi.org/10.1016/j.jics.2022.100498
[23] H. Rao, W. Li, Z. Luo, H. Liu, L. Zhu, and H. Chen, Journal of Materials Research and Technology, **30**, 3079 (2024). https://doi.org/10.1016/j.jmrt.2024.04.008
[24] R. Li, Q. Chu, and J. Liang, Rsc Advances, **5**, 44933 (2015). https://doi.org/10.1039/C5RA05918F
[25] B. Scharifker, and G. Hills, Electrochimica Acta, **28**, 879 (1983). https://doi.org/10.1016/0013-4686(83)85163-9
[26] M.R. Khelladi, L. Mentar, A. Azizi, F. Kadirgan, G. Schmerber, and A. Dinia, Applied surface science. **258**, 3907-3912 (2012). https://doi.org/10.1016/j.apsusc.2011.12.060
[27] A. Mashreghi, and H. Zare, Current Applied Physics, **16**, 599 (2016). https://doi.org/10.1016/j.cap.2016.03.008
[28] X. Cao, H. Wang, T. Liu, Y. Shi, and X. Xue, Materials, **16**, 415 (2023). https://doi.org/10.3390/ma16010415
[29] L. Mentar, Ionics, **18**, 223 (2012). https://doi.org/10.1007/s11581-011-0602-y
[30] J. Bahar, Y. Lghazi, B. Youbi, M. Ait Himi, C. El Haimer, A. Ouedrhiri, A. Aynaou, and I. Bimaghra, Materials Today: Proceedings, **66**, 187 (2022). https://doi.org/10.1016/j.matpr.2022.04.445

[31] A. El-Shaer, S. Ezzat, M.A. Habib, O.K. Alduaij, T.M. Meaz, and S.A. El-Attar, Crystals, **13**, 788 (2023). https://doi.org/10.3390/cryst13050788
[32] D. Abou-Ras, G. Kostorz, A. Romeo, D. Rudmann, and A.N. Tiwari, Thin Solid Films, **480**, 118 (2005). https://doi.org/10.1016/j.tsf.2004.11.033
[33] A.A. Ojo, and I.M. Dharmadasa, Coatings. **9**, 370 (2019). https://doi.org/10.3390/coatings9060370
[34] S.W. Pawar, V.A. Tabhane, P.E. Lokh, F. Khan, J. Kaur, A. Al-Ahmed, and H.M. Pathan, ES Energy & Environment, **17**, 106 (2022). https://doi.org/10.30919/esee8c652

ВПЛИВ БОРНОЇ ТА ЩАВЛЕВОЇ КИСЛОТИ НА МЕХАНІЗМ ЗАРОДЖЕННЯ, СКЛАД, МОРФОЛОГІЮ ТА СТРУКТУРУ ЕЛЕКТРООСАДЖЕНИХ НІКЕЛЕВИХ ПЛІВОК

Ф.З.К. Хамді[1], А. Рахмані[1,2], А. Хамді[1]

[1]*Лабораторія фізичної хімії матеріалів (LPCM), Факультет наук, Університет Амар Теліджі, 03000, Лагуат, Алжир*
[2]*Лабораторія MONARIS, UMR 8233, Університет Сорбонни, 4-та площа Жюссьє, 75005 Париж, Франція*

Тонкі нікелеві плівки були електроосаджені на мідні підкладки за кімнатної температури з використанням водного електроліту, що містить сульфат нікелю, хлорид нікелю та сульфат натрію. Вплив двох добавок (борної кислоти та щавлевої кислоти) на механізм зародження, кристалографічну структуру, морфологію поверхні та хімічний склад отриманих плівок Ni було систематично досліджено за допомогою циклічної вольтамперометрії (CV), хроноамперометрії (CA), рентгенівської дифракції (XRD), скануючої електронної мікроскопії (SEM) та енергодисперсійної рентгенівської спектроскопії (EDS). CV-аналіз показав, що присутність добавок зміщує потенціали катодних піків у бік більш негативних значень, що свідчить про гальмівний ефект відновлення нікелю. Хроноамперометричні дослідження підтвердили, що осадження Ni відбувалося в тривимірному режимі миттєвого зародження, на яке не впливали добавки. Рентгенограми показали, що всі плівки Ni мали гранецентровану кубічну (FCC) структуру з сильною орієнтацією (111), тоді як SEM-зображення вказували на щільнішу та однорідніщу морфологію поверхні за наявності добавок. EDS-аналіз підтвердив присутність Ni у всіх зразках.

Ключові слова: *нікель; електроосадження; добавки; борна кислота; щавлева кислота; зародження*